



Effective removal of brilliant green from aqueous solution with magnetic Fe₃O₄@SDBS@LDHs composites

Dan ZHANG, Ming-yue ZHU, Jin-gang YU, Hui-wen MENG, Fei-peng JIAO

School of Chemistry and Chemical Engineering, Central South University, Changsha 410083, China

Received 8 September 2016; accepted 20 April 2017

Abstract: The magnetic composite-materials (Fe₃O₄@SDBS@LDHs) were prepared by sodium dodecyl benzene sulfonate (SDBS) modified layered double hydroxides (SDBS@LDHs) with Fe₃O₄ via co-precipitation method. The results of XRD, FT-IR and SEM/EDS indicated that the dispersibility of LDHs was improved, and the modification of SDBS took place on the surface of LDHs. The adsorption capacity of Fe₃O₄@SDBS@LDHs to brilliant green (BG) reaches 329.1 mg/g after the adsorption equilibrium. The thermodynamic parameters indicated that the adsorption process was endothermic and spontaneous, and the rate of a reaction increased with the raise of the reaction temperature. The Langmuir model was applicable for describing the sorption isotherms, indicating that the adsorption process is a monolayer adsorption. The results of kinetics study showed that adsorption fitted the pseudo-second order model well. The adsorbents still have good adsorption performance after four adsorption cycles. Moreover, the magnetic composite could be easily separated from aqueous solution. This indicated that Fe₃O₄@SDBS@LDHs can be considered as potential adsorbents in environmental applications for the removal of BG from aqueous solutions.

Key words: layered double hydroxides; sodium dodecyl benzene sulfonate; brilliant green; magnetic materials; adsorption

1 Introduction

Dyes are widely used in various industries, such as textile, leather, paper, cosmetics, and plastics. However, the dye pollutants discharged into rivers and lakes without any prior treatment have caused potential threat to the eco-environment and difficulty to be treated because of large volume, high content of organic dye pollutants [1,2]. Therefore, many efforts have been made to develop effective methods for the elimination of organic dyes from wastewater, including sedimentation, coagulation, flocculation, chemical treatments, oxidation, photodegradation, biological treatments, adsorption, and membrane process [3–6]. Among these methods, adsorption is one of the most commonly used methods due to its operational simplicity, effectiveness, low energy requirements and low cost [7]. Overall, in consideration of environmental problems and economic cost, to develop novel adsorbents with high adsorption efficiency and capacities is necessary and desirable.

Layered double hydroxides (LDHs), are known as hydrotalcitelike compound or anionic clay. LDHs consist of positively charged metal hydroxide layers separated

by anions and water molecules, which are generally expressed as $[M_{1-x}^{2+}M_x^{3+}(\text{OH})_2]^{x+}(A^{n-})_{x/n} \cdot m\text{H}_2\text{O}$, where M^{2+} is a divalent metal cation such as Mg^{2+} , Zn^{2+} , Co^{2+} , Ni^{2+} and Cu^{2+} ; M^{3+} represents a trivalent metal cation such as Al^{3+} , Fe^{3+} and Cr^{3+} ; A^{n-} is the interlayer exchangeable anion, and x is denoted as the molar ratio of $M^{3+}/(M^{2+}+M^{3+})$ generally ranging between 0.20 and 0.33 for pure LDH formation [8,9]. The excellent interlayer anion-exchange capacity, high layer charge density, and large specific surface area allow LDHs to become effective adsorbents to adsorb anionic dyes in aqueous solutions [10,11]. Recently, the modification of LDHs has been focused on increasing the adsorption capacity due to their potential application as special adsorbents for organic contaminants [12]. Intercalation of organic phase composite is one of the popular ways of modification, such as sodium dodecyl sulfate and quaternary ammonium salts [13].

Though LDHs have good adsorbing ability to dyes their poor separation efficiency in aqueous solution still influenced their application in industry. In recent years, magnetic separation technology has attracted much attention for its simple separation method and high separation efficiency. Therefore, it is necessary to

enhance separation efficiency and re-dispersion performance of LDHs in the aqueous solution by combining Fe₃O₄ nanoparticle and LDH [14]. YAN et al [15] fabricated three different magnetic core-shell Fe₃O₄@LDHs composites via a rapid coprecipitation method to apply for wastewater treatment.

Herein, we developed a facile two-step approach for the synthesis of magnetic Fe₃O₄@SDBS@LDHs composites. The synthesized composites were characterized using XRD, FT-IR, SEM/EDS and UV–Vis. Batch experiments were conducted to study the adsorption efficiency of brilliant green (BG). The effects of the initial concentration of the composites, pH and contact time on BG adsorption were investigated. In addition, the kinetics and thermodynamics of the adsorption process were also studied. The results showed that the Fe₃O₄@SDBS@LDHs can serve as efficient and low-cost adsorbents for the removal of BG from wastewater.

2 Experimental

2.1 Materials

Mg(NO₃)₂·6H₂O, Al(NO₃)₃·9H₂O and sodium dodecyl benzene sulfonate(SDBS) were purchased from Fengchuan Chemical Reagent Co., Ltd., Tianjin, China. FeCl₂·6H₂O, FeCl₃·6H₂O, NaOH and ammonia were received from Sinopharm Chemical Reagent Co., Ltd. BG was obtained from Shanghai Chemical Reagent Station. All the reagents were analytical grade chemicals and used without any purification.

2.2 Synthesis of SDBS@LDHs

The SDBS@LDHs were prepared by a co-precipitation method [16]. Mg(NO₃)₂·6H₂O and Al(NO₃)₃·9H₂O were dissolved completely in deionized water to obtain metal salt solutions. An alkaline solution with 2.0 mol/L NaOH was added into the solution under vigorous stirring in N₂ flow to modulate the pH 10. Then, 100 mL of 0.015 mol/L SDBS solution was added into the above mixture solution and the mixture solution was aged at 80 °C for 9 h in a thermostatic bath. Finally, the obtained white precipitate was then centrifuged, washed thoroughly with deionized water until neutral pH and dried at 60 °C overnight.

2.3 Synthesis of magnetic Fe₃O₄@SDBS@LDHs

The Fe₃O₄ nanoparticles were synthesized by co-precipitation method [17]. 0.02 mol of FeCl₃·6H₂O and 0.01 mol of FeCl₂·4H₂O were dissolved in 100 mL of deaeration water. Afterwards, this mixture solution was transferred into a 100 mL three-necked flask. An alkaline solution including a certain amount of NH₃·H₂O was added into the mixed solution under stirring to keep

the pH at about 10 and the mixture solution was continuously stirred at 80 °C for 0.5 h. At the end, the resulting slurry was separated by centrifugation, washed with deaeration water several times and dried at 60 °C for 24 h.

The magnetic Fe₃O₄@SDBS@LDHs composites were prepared by hydrothermal synthesis method. The prepared Fe₃O₄ (0.5 g) and SDBS@LDHs (1.0 g) were ultrasonically dispersed into 80 mL distilled water to obtain a uniform suspension. Afterwards, this mixture solution was transferred into a 100 mL Teflon-lined stainless steel autoclave and kept at 120 °C for 4 h. Finally, after cooling to the ambient temperature naturally, the obtained white precipitate was centrifuged, washed thoroughly with deionized water three times and dried in a vacuum oven at 60 °C for 24 h.

2.4 Characterization methods

XRD patterns were obtained by using Rigaku D/MAX 2500 X-ray diffractometer (Rigaku, Tokyo) with Cu K_α radiation (40 kV, 250 mA, λ=0.154 nm) to confirm the structure of the material. The 2θ angle of the diffractometer was stepped from 3° to 70° at a scan rate of 8 (°)/min. UV–Vis absorption spectra of the samples were recorded on a Lambda 950 UV–Vis spectrophotometer (PerkinElmer, USA). FT-IR spectra were obtained using a NICOLET AVATAR 360 FT-IR spectrophotometer by the standard KBr disk method. FTIR spectra were recorded in the spectral range of 4000–400 cm⁻¹ on Spectrum One FTIR spectrometer (Thermo-Nicolet, USA). The size and morphology of the samples were examined by scanning electron microscopy (SEM) using a TESCAN MIRA3 LMU microscope, combined with energy-dispersive spectroscopy (EDS) for the determination of the chemical composition.

2.5 Adsorption experiments

Adsorption experiments were carried out in conical flasks. A series of 20 mL BG solutions from 50 to 120 mg/L were prepared in advance. 10 mg adsorbents were added to every BG solution. The initial pH of solution (4, 5, 6, 7, 8, 9) was adjusted by dropwise adding HCl or NaOH solution. The batch experiments for adsorption isotherm of BG were also carried out at varying temperatures (293, 298, and 303 K) with different initial concentrations. The solution and phase after equilibrium were separated by an external magnet. The residual BG concentrations in the sample solutions were determined by the UV–Vis spectrophotometer at 626 nm. The adsorption amount (Q_t) and removal efficiency (η) were calculated by the following equations [18]:

$$Q_t = \frac{C_0 - C_e}{m} \times V \quad (1)$$

$$\eta = \frac{C_0 - C_e}{C_0} \times 100\% \quad (2)$$

where C_0 (mg/L) and C_e (mg/L) are the initial and equilibrium concentrations of BG, respectively, V (L) is the volume of the dye and m (g) denotes the mass of the adsorbents used.

3 Results and discussion

3.1 Characterization of samples

X-ray diffraction patterns of LDHs, SDBS@LDHs, Fe_3O_4 and Fe_3O_4 @SDBS@LDHs composites are illustrated in Fig. 1. The peaks of SDBS@LDHs located at (003), (006), (009), and (110) were attributed to the characteristic peaks of pure LDHs [19,20]. SDBS@LDHs had no significant changes in the interlayer space compared to the pure LDHs. This unchanged “gallery height” indicated that the SDBS did not intercalate the interlayers and the modification of SDBS took place on the surface of LDHs. Magnetic Fe_3O_4 @SDBS@LDHs composites had the characteristic peaks of pure LDHs and Fe_3O_4 , but the intensities of the characteristic reflections of the pure LDHs phases were obviously reduced compared to those in pure LDHs.

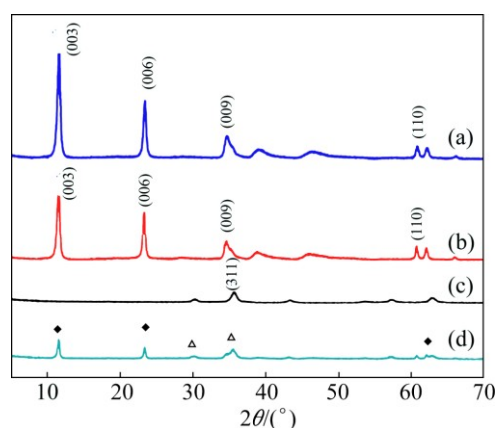


Fig. 1 XRD patterns of LDHs (a), SDBS@LDHs (b), Fe_3O_4 (c) and Fe_3O_4 @SDBS@LDHs (d)

The morphologies of the as-prepared products were characterized by SEM. The SEM images and EDX spectrum of those samples are shown in Fig. 2. We could find that pure LDHs have obvious hexagonal lamellar structures and 10–100 nm in particle size from Fig. 2(b). As seen in Fig. 2(c), SDBS@LDHs still had hexagonal lamellar structures, which indicated that SDBS did not change the structure of the LDH and improve agglomeration between the particles. As shown in Fig. 2(a), the prepared Fe_3O_4 was nanometer microspheres with uniform particle size and high purity. After combining with SDBS@LDHs, the surface of Fe_3O_4 @SDBS@LDHs composites was rougher than

that of initial Fe_3O_4 (Fig. 2(d)). The corresponding EDX spectrum (Fig. 2(e)) confirmed that Fe_3O_4 @SDBS@LDHs composites were composed of C, S, O, Fe, Mg and Al.

The optical absorption spectra of Fe_3O_4 @SDBS@LDHs and Fe_3O_4 @LDHs were examined by UV–Vis diffuse reflectance spectroscopy. As shown in Fig. 3, in the ultraviolet region and visible region, the absorption of the Fe_3O_4 @SDBS@LDHs is obviously higher than that of Fe_3O_4 @LDHs, which can be ascribed to the formation of the SDBS@LDHs. The SDBS on the LDHs surface could cause the best absorbability in the ultraviolet and visible light.

The FT-IR spectra of the magnetic Fe_3O_4 @SDBS@LDHs composites are shown in Fig. 4. The intense broadband around 3400 cm^{-1} was associated with stretching of O—H and water molecules existing in the sample. The bands at 1630 and 1468 cm^{-1} were due to the water molecules and C—H bending vibration [21]. The peaks at 580 and 2850 cm^{-1} were due to the vibration absorption of Fe—O lattice mode and —CH₃, respectively. The absorption peaks in the 1600 – 1400 cm^{-1} region were derived from the benzene skeleton vibration. Moreover, for the SDBS (Fig. 4(a)), the band corresponding to the S=O asymmetric vibration was recorded at 1085 cm^{-1} . But the absorption band observed around 1059 cm^{-1} corresponded to the S=O stretching vibration of the Fe_3O_4 @SDBS@LDH and SDBS@LDH composites, because the original structure of the S=O was destroyed in the synthesis process of composite materials [22]. This phenomenon indicated that the interaction force between particles was strengthened, further explaining that hydrogen bonding exists in the forms of S=O—H—O—M (M=Mg or Al) between hydroxyl laminates and surface active anions.

3.2 Effect of contact time on BG adsorption

An evaluation of the BG (80 mg/L, 150 mL) adsorbed on the Fe_3O_4 @SDBS@LDHs (20 mg) at 293 K without pH control as a function of adsorption time is presented in Fig. 5. BG adsorption rate increased rapidly in the first 200 min, then increased slowly and reached adsorption equilibrium at about 600 min. After reaching equilibrium, the adsorption capacity of Fe_3O_4 @SDBS@LDHs to BG was evaluated as 329.1 mg/g.

3.3 Effect of initial solution pH on BG adsorption

The influence of solution pH on the removal of BG by magnetic Fe_3O_4 @SDBS@LDHs composites was studied at different initial pH values ranging from 4.0 to 9.0 at 25 °C, initial BG concentration (100 mg/L), dye volume (50 mL) and adsorbent dose (10 mg) and the results are depicted in Fig. 6. Along with the further increase of pH value, there was a sharp increase of

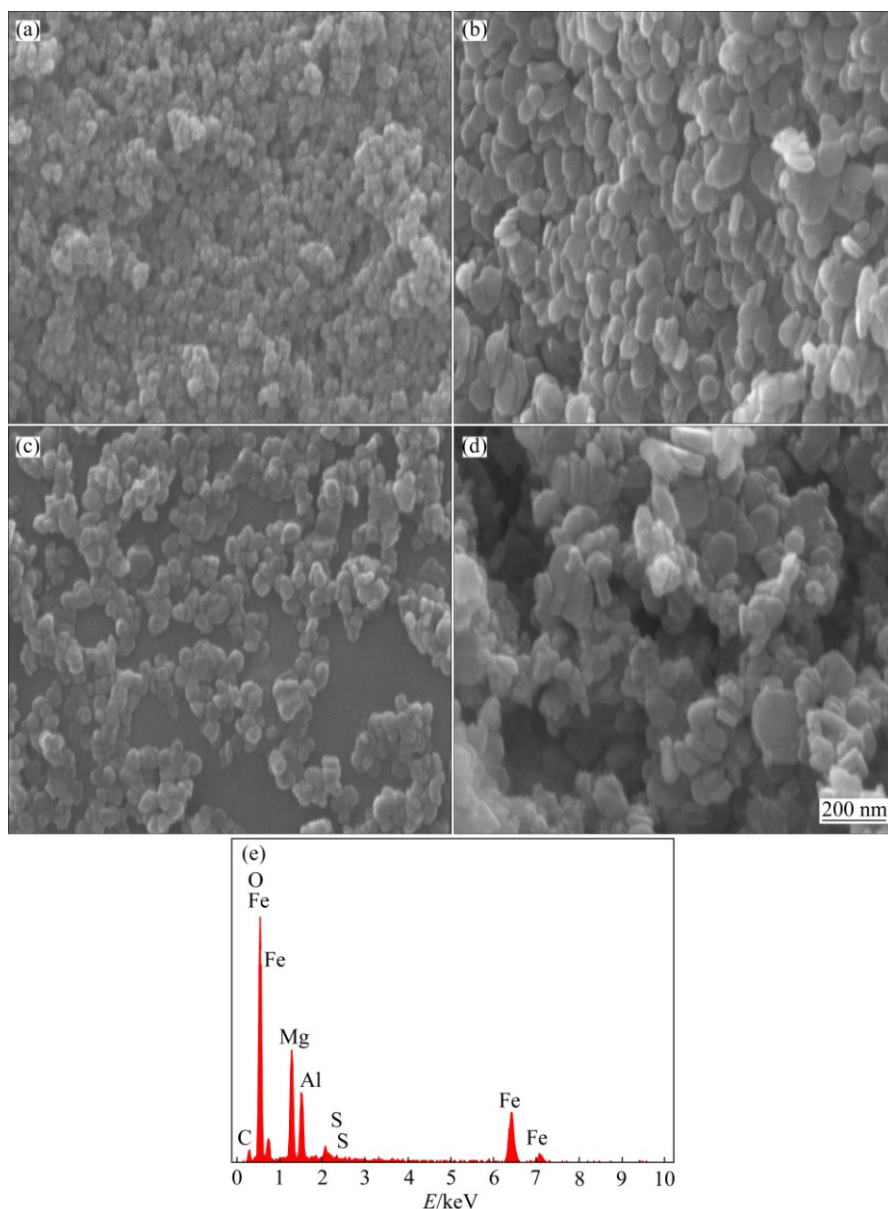


Fig. 2 SEM images of Fe₃O₄ (a), LDHs (b), SDBS@LDHs (c), Fe₃O₄@SDBS@LDHs (d) and EDX spectrum from Fe₃O₄@SDBS@LDHs (e)

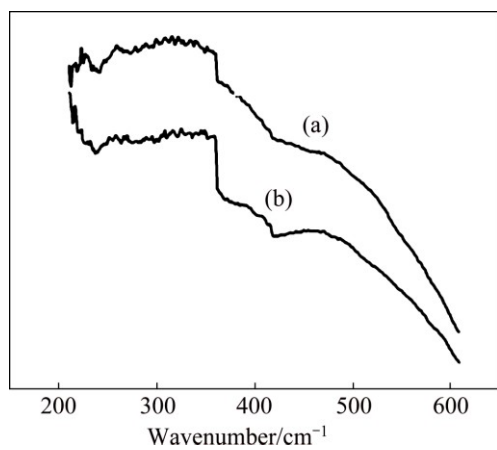


Fig. 3 UV-Vis absorption spectra of Fe₃O₄@SDBS@LDHs (a) and Fe₃O₄@LDHs (b)

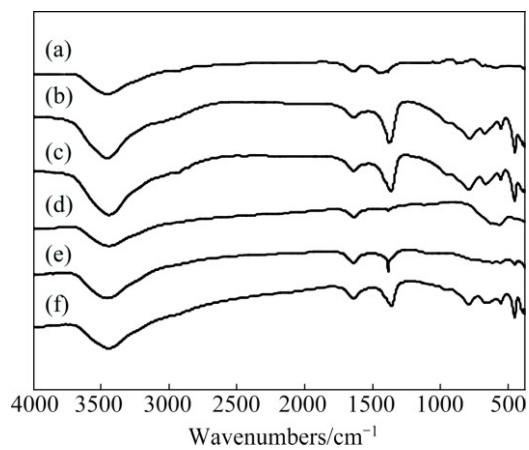


Fig. 4 FT-IR spectra of SDBS (a), LDHs (b), SDBS@LDHs (c), Fe₃O₄ (d), Fe₃O₄@LDHs (e) and Fe₃O₄@SDBS@LDHs (f)

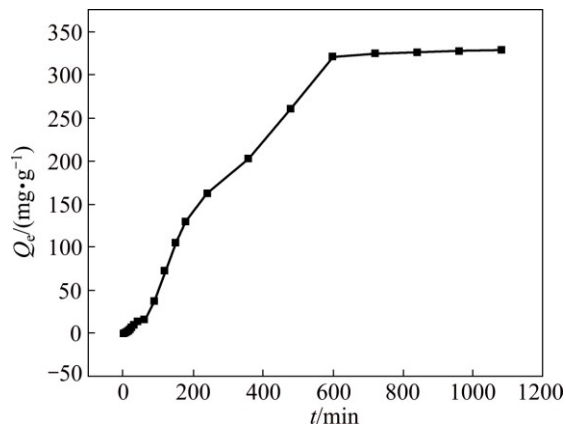


Fig. 5 Effect of contact time on adsorption ability of $\text{Fe}_3\text{O}_4@\text{SDBS}@\text{LDHs}$ composites

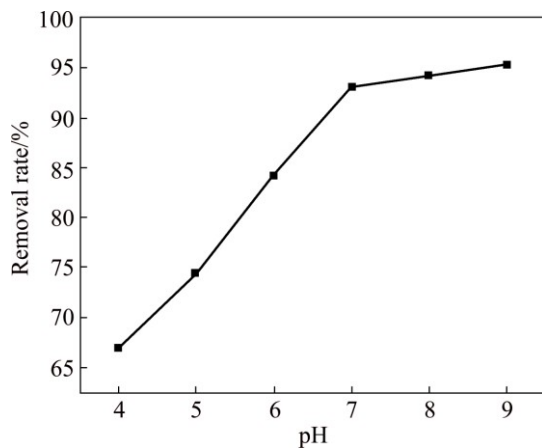


Fig. 6 Effect of solution pH on BG adsorption by $\text{Fe}_3\text{O}_4@\text{SDBS}@\text{LDHs}$ composites

removal rate, and then stabilized at pH of 7–9. From this result, we could find that $\text{Fe}_3\text{O}_4@\text{SDBS}@\text{LDHs}$ adsorbed BG due to electrostatic attraction between anionic surfactant modified LDHs and cationic dye. When the solution was acid, lots of H^+ ions were present in the solution, and could form competitive forces with positively charged cationic dye, so effective absorption decreased for the removal of BG from aqueous solution.

3.4 Effect of initial concentration on BG adsorption

The influence of BG (50 mL) adsorbed on the $\text{Fe}_3\text{O}_4@\text{SDBS}@\text{LDHs}$ (10 mg) at different BG initial concentrations was investigated at neutral pH and different temperatures (293, 298 and 303 K) and the results are given in Fig. 7. The adsorption capacities of samples showed the rising trend and representative linear curves with the initial BG concentration. The adsorption capacities increased for BG as the temperature increased.

3.5 Adsorption isotherms

The adsorption isotherms of BG on magnetic $\text{Fe}_3\text{O}_4@\text{SDBS}@\text{LDHs}$ composite were measured at three

different temperatures. The Langmuir and Freundlich models, expressed as follows (Eqs. (3) and (4), respectively) are the most frequently used equations for fitting the experimental data of an isotherm:

$$\frac{C_e}{Q_e} = \frac{1}{k_a Q_m} + \frac{C_e}{Q_m} \quad (3)$$

$$\ln Q_e = \ln k_f + (1/n) \ln C_e \quad (4)$$

where Q_e (mg/g) is the adsorption capacity at equilibrium, Q_m (mg/g) is the maximum adsorption capacity, k_f and n are the Freundlich temperature-dependent constants, and the $1/n$ value in the range of 0.1–1 indicates a favorable adsorption process and intensity of the adsorption; and k_a (L/mg) is the Langmuir constant related to adsorption energy.

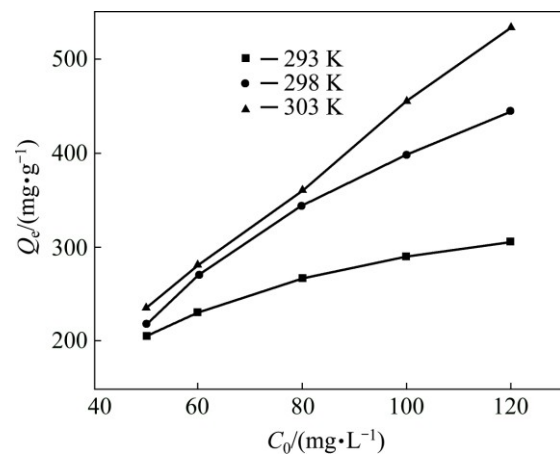


Fig. 7 Effect of initial BG concentration on adsorption ability of $\text{Fe}_3\text{O}_4@\text{SDBS}@\text{LDHs}$ composites

The adsorption isotherms of BG onto $\text{Fe}_2\text{O}_3@\text{SDBS}@\text{LDHs}$ are shown in Fig. 8. Typical parameter values obtained by linear curve fitting are listed in Table 1. According to the values of R^2 , the Langmuir model is more suitable than the Freundlich model to describe the adsorption of BG at different temperatures, indicating that the adsorption process is a monolayer adsorption [23].

3.6 Adsorption thermodynamics

The study of the temperature effect on BG adsorption by $\text{Fe}_3\text{O}_4@\text{SDBS}@\text{LDHs}$ enabled us to determine the thermodynamic parameters such as Gibbs free energy (ΔG), standard enthalpy (ΔH) and standard entropy change (ΔS) of these reactions by using the following equations:

$$\Delta G = -RT \ln k_d \quad (5)$$

$$\Delta H = \Delta G + T\Delta S \quad (6)$$

$$\ln k_d = \Delta S/R - \Delta H/(RT) \quad (7)$$

where T is the temperature (K), R (8.314 J/(mol·K)) is

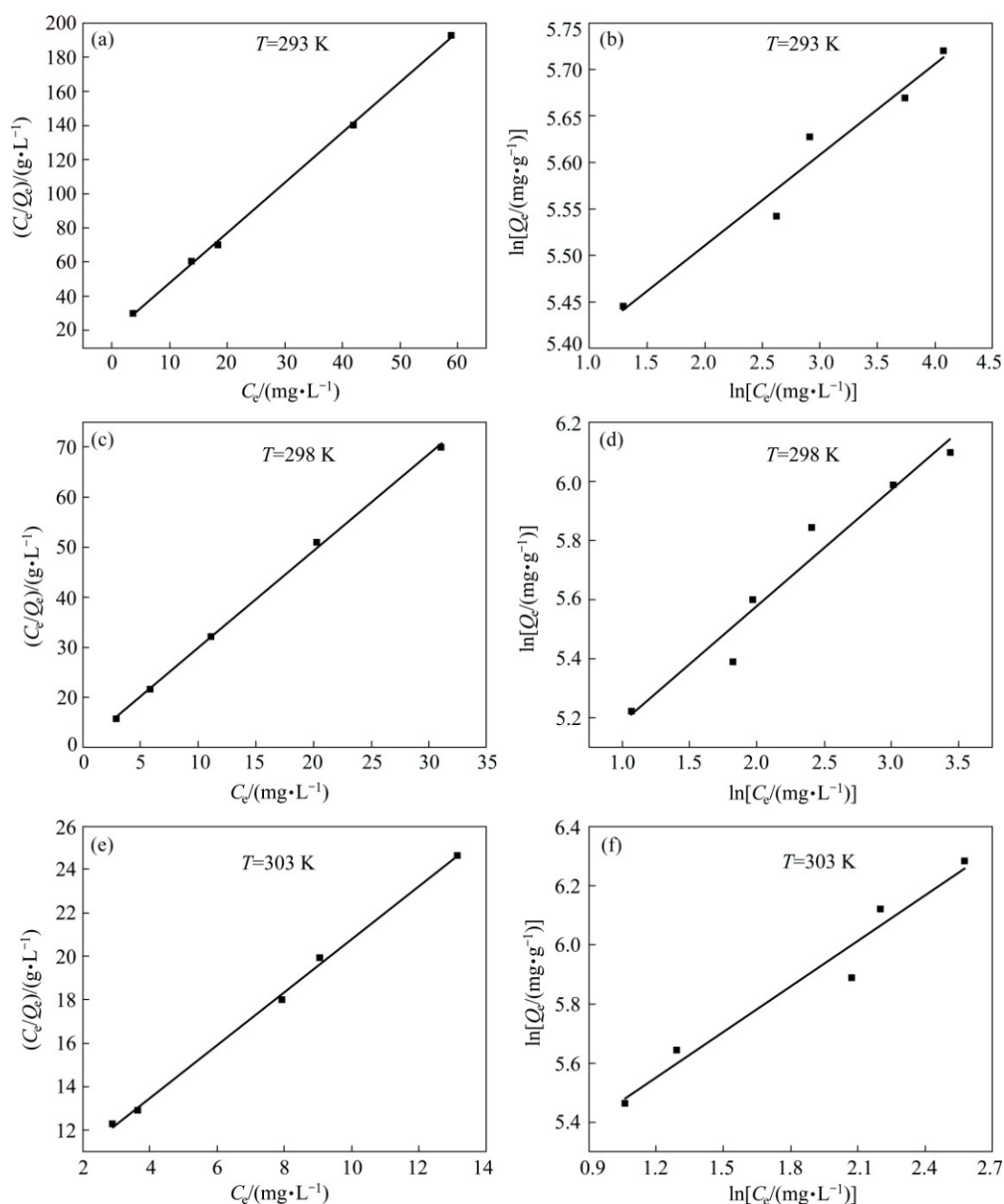


Fig. 8 Adsorption isotherms of BG on magnetic $\text{Fe}_3\text{O}_4@\text{SDBS}@\text{LDHs}$ composites: (a, c, e) Langmuir model; (b, d, f) Freundlich model

Table 1 Parameters of Freundlich and Langmuir isotherms for adsorption of dyes onto $\text{Fe}_3\text{O}_4@\text{SDBS}@\text{LDHs}$ composites

T/K	Langmuir model			Freundlich model		
	$Q_m/(\text{mg}\cdot\text{g}^{-1})$	$k_a/(\text{L}\cdot\text{mg}^{-1})$	R^2	k_f	n	R^2
293	340.1	0.16	0.9989	202.97	10.17	0.9493
298	518.1	0.18	0.9985	120.47	2.54	0.9397
303	819.6	1.00	0.9975	138.62	1.94	0.9470

the mole gas constant. The plot of $\ln k_d$ against $1/T$ gives a straight line, and the slope and the intercept correspond to $\Delta H/R$ and $\Delta S/R$, respectively.

The thermodynamic parameters (ΔG , ΔH , and ΔS)

for the adsorption of BG on $\text{Fe}_3\text{O}_4@\text{SDBS}@\text{LDH}$ are presented in Table 2. The obtained negative values of ΔG at different temperatures indicated that the adsorption of BG was thermodynamically feasible and spontaneous in

nature. The positive value of ΔH confirmed the endothermic nature of BG adsorption. The values of ΔG decreased from -4.0067 to -9.0259 kJ/mol, indicating that the endothermic adsorption of BG was enhanced by an increase in temperature. In general, ΔH value between 5 and 40 kJ/mol corresponds to physical adsorption and that between 40 and 800 kJ/mol corresponds to chemical adsorption [24]. Conclusion could be made that the adsorption process was mainly a chemical adsorption process at $40 \text{ kJ/mol} < \Delta H < 800 \text{ kJ/mol}$. The positive value of ΔS suggested the increased randomness at the solid/solution interface in this system.

Table 2 Thermodynamic data for adsorption of BG onto $\text{Fe}_3\text{O}_4@\text{SDBS}@LDH$

T/K	$\Delta G/(\text{kJ}\cdot\text{mol}^{-1})$	$\Delta H/(\text{kJ}\cdot\text{mol}^{-1})$	$\Delta S/(\text{kJ}\cdot\text{mol}^{-1}\cdot\text{K}^{-1})$
293	-4.0067		
298	-6.4821	152.1	532.6
303	-9.0259		

3.7 Adsorption kinetics

Adsorption kinetic studies are important to evaluate the effectiveness of an adsorbent and to provide valuable insights into the mechanism of adsorption reactions. The pseudo-first-order kinetics equation is expressed in the form:

$$\ln(Q_e - Q_t) = \ln Q_e - k_1 t \quad (8)$$

The pseudo-second-order kinetic equation is expressed as

$$\frac{t}{Q_t} = \frac{1}{k_2 Q_e^2} + \frac{t}{Q_e} \quad (9)$$

where Q_t (mg/g) and Q_e (mg/g) are respectively the amounts of adsorbed BG at time t and equilibrium, k_1 is the rate constant of the first-order, and k_2 is the rate constant of pseudo-second-order for the adsorption.

The intraparticle diffusion model is a single-resistance model in nature and has been applied to describing adsorption systems previously. The expression for this model is

$$Q_t = k_p t^{1/2} + C \quad (10)$$

From Fig. 9, it can be seen that pseudo-second order kinetic model is in good agreement with the experimental data in the entire adsorption range. So, the pseudo-second-order kinetic model better represented the adsorption kinetics, indicating that the chemisorption is a rate-limited process. Linear profile was obtained for intraparticle diffusion model plot and this plot did not pass through the origin (Fig. 9(c)), which suggested that boundary layer diffusion also occurred in the uptake of BG onto $\text{Fe}_3\text{O}_4@\text{SDBS}@LDH$ s composites.

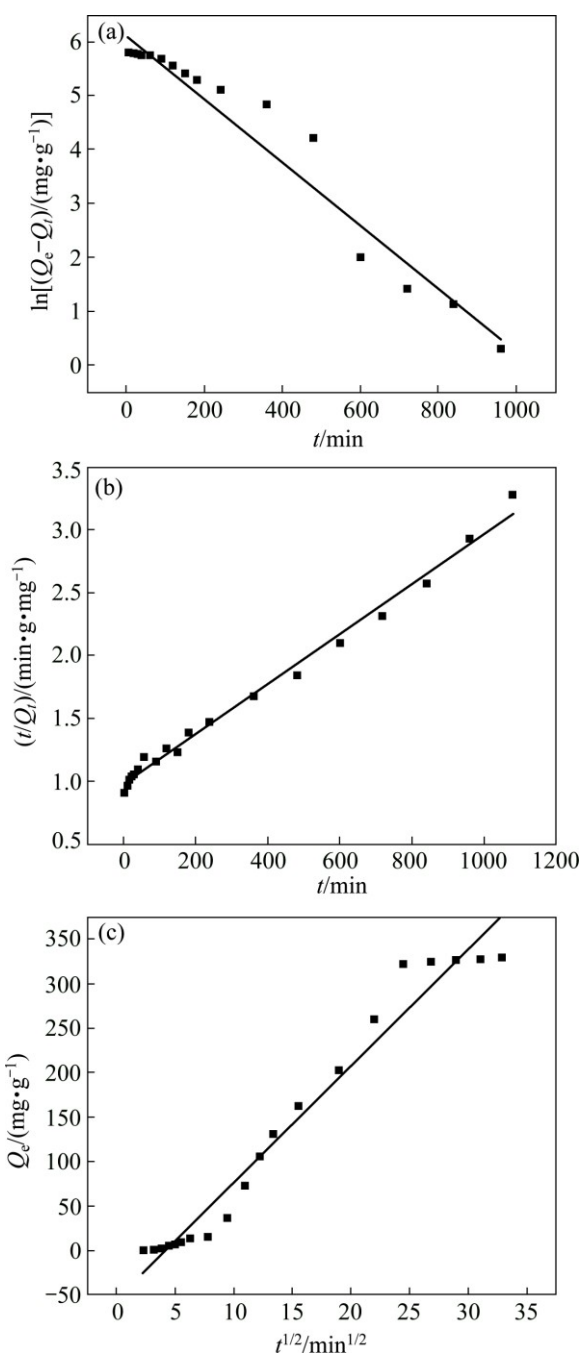


Fig. 9 Adsorption kinetic curves of first-order kinetic model (a), second-order kinetic model (b), and intraparticle diffusion model (c)

3.8 Recycling of adsorbents

The development of reusable adsorbent is economically important. By shaking with adding the lye to the adsorbents, adsorbed BG can be almost eliminated and removed, and thus the adsorbents can be reconverted as adsolubilization materials for reuse. Consecutive adsolubilization-regeneration cycles for BG with the $\text{Fe}_3\text{O}_4@\text{SDBS}@LDH$ adsorbents were repeated 4 times under the same experimental conditions. Figure 10 showed that, a deterioration of the $\text{Fe}_3\text{O}_4@\text{SDBS}@LDH$

adsorption capacity (76%) could be observed during the second use, BG removal rates still remained more than 60% after four cycles. This may be attributed to the fact that it was unavoidable to lose some adsorbents during the consecutive adsorption–desorption cycles. These results suggested that $\text{Fe}_3\text{O}_4@\text{SDBS}@\text{LDH}$ adsorbent could be reusable for multiple adsorption cycles.

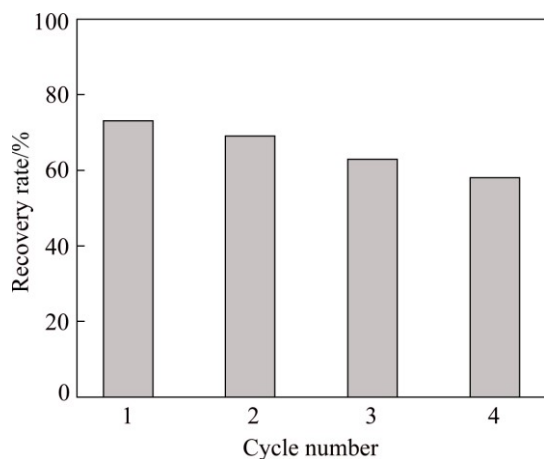


Fig. 10 Recycling experiment with four cycles of removing BG by magnetic $\text{Fe}_3\text{O}_4@\text{SDBS}@\text{LDH}$ s composites

4 Conclusions

1) The magnetic $\text{Fe}_3\text{O}_4@\text{SDBS}@\text{LDH}$ s composites were prepared by SDBS modified LDH (SDBS@LDHs) with Fe_3O_4 via co-precipitation method. The results of XRD, FT-IR and SEM/EDS indicated that the dispersibility of LDHs was improved, and the modification of SDBS took place on the surface of LDHs.

2) The optimum adsorption capacity reached 329.1 mg/g under neutral condition at room temperature. The $\text{Fe}_3\text{O}_4@\text{SDBS}@\text{LDH}$ s have high adsorption capacity due to electrostatic attraction between anionic surfactant modified LDHs and cationic dye. The kinetic model fitted well with the pseudo-second order, and the isotherm obeyed the Langmuir model better than Freundlich model. Besides, adsorption process of BG on $\text{Fe}_3\text{O}_4@\text{SDBS}@\text{LDH}$ s was spontaneous endothermic chemisorptions according to the thermodynamic study. BG removal rate still remained more than 60% after four adsorption cycles.

References

[1] ABDERRAIEK K, KAOUTHER A, NAJOUA F S, SRASRA E. Synthesis and characterization of [Zn–Al] LDH: Study of the effect of calcination on the photocatalytic activity [J]. *Applied Clay Science*, 2016, 119: 229–235.

[2] MA J, DING J, YU L, KONG Y, KOMARNENI S, MONAQUEL S, SHENG J, WANG X K, LI H, HUANG Y Y. BiOCl dispersed on NiFe–LDH leads to enhanced photodegradation of Rhodamine B dye

[J]. *Applied Clay Science*, 2015, 109: 76–82.

[3] FORGACS E, CSERHATI T, OROS G. Removal of synthetic dyes from wastewater: A review [J]. *Environment International*, 2004, 30(7): 953–971.

[4] GOLOB V, VINDER A, SIMONIC M. Efficiency of the coagulation/flocculation method for the treatment of dyebath effluents [J]. *Dyes and Pigments*, 2005, 67(2): 93–97.

[5] WEI J, ZHU R, ZHU J, GE F, YUAN P, HE H, MING C. Simultaneous sorption of crystal violet and 2-naphthol to bentonite with different CECs [J]. *Journal of Hazardous Materials*, 2009, 166(1): 195–199.

[6] ZHANG L, DAI C H, ZHANG X X, LIU X X, YAN J H. Synthesis and highly efficient photocatalytic activity of mixed oxides derived from ZnNiAl layered double hydroxides [J]. *Transactions of Nonferrous Metals Society of China*, 2016, 26(9): 2380–2389.

[7] WU X, JIA W. Biomass-derived multifunctional magnetite carbon aerogel nanocomposites for recyclable sequestration of ionizable aromatic organic pollutants [J]. *Chemical Engineering Journal*, 2014, 245: 210–216.

[8] EVANS D G, SLADE R C T. Structural aspects of layered double hydroxides [J]. *Structure and Bonding*, 2006, 119: 1–87.

[9] LONG Y L, YU J G, JIAO F P, YANG W J. Preparation and characterization of MWCNTs/LDHs nanohybrids for removal of Congo red from aqueous solution [J]. *Transactions of Nonferrous Metals Society of China*, 2016, 26(10): 2701–2710.

[10] AI L H, ZHANG C Y, MENG L Y. Adsorption of methyl orange from aqueous solution on hydrothermal synthesized Mg–Al layered double hydroxide [J]. *Journal of Chemical & Engineering Data*, 2011, 56(11): 4217–4225.

[11] ZAGHOUEANE-BOUDIAF H, BOUTAHALA M, ARAB L. Removal of methyl orange from aqueous solution by uncalcined and calcined MgNiAl layered double hydroxides (LDHs) [J]. *Journal of Chemical & Engineering Data*, 2012, 187: 142–149.

[12] RUAN X X, CHEN Y H, CHEN X, QIAN G R, FROST R. Sorption behavior of methyl orange from aqueous solution on organic matter and reduced graphene oxides modified Ni–Cr layered double hydroxides [J]. *Chemical Engineering Journal*, 2016, 297: 295–303.

[13] ZAGHOUEANE-BOUDIAF H, BOUTAHALA M, TIAR C, TIAR C, ARAB L, GARIN F. Treatment of 2,4,5-trichlorophenol by MgAl–SDBS organo-layered double hydroxides: Kinetic and equilibrium studies [J]. *Chemical Engineering Journal*, 2011, 173(1): 36–41.

[14] CHEN D, LI Y, ZHANG J, ZHOU J Z, GUO Y, LIU H. Magnetic $\text{Fe}_3\text{O}_4/\text{ZnCr}$ -layered double hydroxide composite with enhanced adsorption and photocatalytic activity [J]. *Chemical Engineering Journal*, 2012, 185: 120–126.

[15] YAN L, YANG K, SHAN R, YAN T, WEI J, YU S J, YU H Q, DU B. Kinetic, isotherm and thermodynamic investigations of phosphate adsorption onto core–shell $\text{Fe}_3\text{O}_4@\text{LDH}$ s composites with easy magnetic separation assistance [J]. *Journal of Colloid and Interface Science*, 2015, 448: 508–516.

[16] XU J F, SHI W, NI Z M, SUN Z Y, QIAN P P. Surface characterization for anionic-nonionic surfactant modified layered double hydroxides [J]. *Chinese Journal of Inorganic Chemistry*, 2014, 30(5): 977–983.

[17] MENG H, ZHANG Z, ZHAO F, ZHAO F X, QIU T, YANG J D. Orthogonal optimization design for preparation of Fe_3O_4 nanoparticles via chemical coprecipitation [J]. *Applied Surface Science*, 2013, 280(8): 679–685.

[18] SHENG G, ALSAEDI A, SHAMMAKH W. Enhanced sequestration of selenite in water by nanoscale zero valent iron immobilization on carbon nanotubes by a combined batch, XPS and XAFS investigation [J]. *Carbon*, 2016, 99: 123–130.

- [19] SHAN R R, YAN L G, YANG Y M, YANG K, YU S J, YU H Q, ZHU B C, DU B. Highly efficient removal of three red dyes by adsorption onto Mg–Al-layered double hydroxide [J]. *Journal of Industrial and Engineering Chemistry*, 2015, 21: 561–568.
- [20] TONG D S, LIU M, LI L, LIN C X, YU W H, XU Z P, ZHOU C H. Transformation of alunite residuals into layered double hydroxides and oxides for adsorption of acid red G dye [J]. *Applied Clay Science*, 2012, 70: 1–7.
- [21] THOMAS G S, RADHA A V, KAMATH P V, KANNAN S. Thermally induced polytype transformations among the layered double hydroxides (LDHs) of Mg and Zn with Al [J]. *The Journal of Physical Chemistry B*, 2006, 110 (25): 12365–12371.
- [22] PALAZZESI F, CALVAARESI M, ZERBETTO F. A molecular dynamics investigation of structure and dynamics of SDS and SDBS micelles [J]. *Soft Matter*, 2011, 7(19): 9148–9156.
- [23] SHUANG C, LI P, LI A, ZHOU Q, ZHANG M, ZHOU Y. Quaternized magnetic microspheres for the efficient removal of reactive dyes [J]. *Water Research*, 2012, 46: 4417–4426.
- [24] TANG H, ZHOU W, ZHANG L. Adsorption isotherms and kinetics studies of malachite green on chitin hydrogels [J]. *Journal of Hazardous Materials*, 2012, 209–210(1): 218–225.

利用磁性复合材料 $\text{Fe}_3\text{O}_4@\text{SDBS}@\text{LDHs}$ 从水溶液中有效去除灿烂绿

张丹, 朱明跃, 于金刚, 孟慧雯, 焦飞鹏

中南大学 化学化工学院, 长沙 410083

摘要: 利用十二烷基苯磺酸钠改性的水滑石 (SDBS@LDHs) 与磁性粒子 Fe_3O_4 共沉淀作用, 得到 $\text{Fe}_3\text{O}_4@\text{SDBS}@\text{LDHs}$ 磁性复合材料。XRD、FT-IR、SEM/EDS 等表征结果表明, $\text{Fe}_3\text{O}_4@\text{SDBS}@\text{LDHs}$ 的分散性得到了提高, SDBS 对 LDHs 的改性在 LDHs 层板表面进行。在吸附平衡后, 磁性复合材料对灿烂绿的吸附量达到 329.1 mg/g。热力学参数表明, 吸附过程为自发吸热反应, 且温度越高, 反应速率越快。吸附过程的热力学符合 Langmuir 等温吸附模型, 属于单分子层吸附; 吸附动力学符合准二级动力学模型。吸附剂在 4 次循环后仍具有较好的吸附能力。此外, 磁性复合物更容易从水溶液中分离。这表明, 在环境应用方面 $\text{Fe}_3\text{O}_4@\text{SDBS}@\text{LDHs}$ 可以作为一种潜在的吸附剂从水溶液中去除灿烂绿。

关键词: 水滑石; 十二烷基苯磺酸钠; 灿烂绿; 磁性材料; 吸附

(Edited by Wei-ping CHEN)